Performance of a permanent-magnet helicon source at 27 and 13 MHz

Francis F. Chen
Electrical Engineering Department, University of California, Los Angeles, California 90095, USA

(Received 19 July 2012; accepted 7 September 2012; published online 26 September 2012)

A small helicon source is used to create dense plasma and inject it into a large chamber. A permanent magnet is used for the dc magnetic field (B-field), making the system very simple and compact. Though theory predicts that better antenna coupling will occur at 27.12 MHz, it was found that 13.56 MHz surprisingly gives even higher density due to practical effects not included in theory. Complete density n and electron temperature T_e profiles are measured at three distances below the source. The plasma inside the source is also measured with a special probe, even under the antenna. The density there is lower than expected because the plasma created is immediately ejected, filling the experimental chamber. The advantage of helicons over inductively coupled plasmas (with no B-field) increases with RF power. At high B-fields, edge ionization by the Trivelpiece-Gould mode can be seen. These results are useful for design of multiple-tube, large-area helicon sources for plasma etching and deposition because problems are encountered which cannot be foreseen by theory alone. © *2012 American Institute of Physics*.
[http://dx.doi.org/10.1063/1.4754580]

I. BACKGROUND

Helicon discharges are known to be good sources of dense plasma for industrial applications, but they normally require a large, heavy electromagnet and its power supply. This disadvantage has been overcome by the invention[1] of permanent-magnet helicon discharges using the remote, reverse field of small annular magnets in combination with the Low-Field Peak[2] in density caused by constructive interference of the reflected backward wave. This effect causes a useful increase in density occurring at a density that depends on the magnetic field and the length of the discharge tube. An array of eight small tubes, built several years ago,[3] successfully produced plasmas of density in the 10^{11} cm^{-3} range, uniform over 56 cm width. That experiment demonstrated that simple, inexpensive helicon arrays can cover large substrates with uniform plasma for roll-to-roll processing. In the present work, one of the helicon sources in the array is studied in detail in a cylindrically symmetric system to see if permanent magnet (PM) helicons can be used for other applications such as spacecraft thrusters or optical coatings. It has been shown[4] that helicon sources can produce an interesting amount of thrust for that purpose, but experiments so far have used large electromagnets for the DC field, and these may be incompatible with the weight limits of spacecraft. The use of PM helicons for thrusters has already been investigated extensively by Takahashi *et al.*[5–7] Their configuration of PMs is quite different from ours and does not use annular magnets. For thruster applications, that work is much more advanced than ours, since the ion energy distributions were measured in detail. The present paper deals instead with the physics of PM helicon discharges and how their design for ejecting plasma has unexpected considerations. Comparisons between 13.56 and 27.12 MHz frequencies and between $B = 0$ and $B > 0$ operation are made.

II. APPARATUS

A. Helicon discharge

The basic source is shown in Fig. 1(a). The B-field is provided by an annular permanent magnet above the discharge tube and can be adjusted by varying its height. The NdFeB magnet has 3-in. (7.6 cm) inner and 5-in. (12.7 cm) outer diameters and is 1 in. (2.54 cm) thick. It is shown at its optimum height. The vertical-probe extension is shown in Fig. 1(b), together with a second magnet which can be added for higher fields. The loop antenna is placed at the bottom to eject the most plasma down into a large chamber. RF frequencies of 27.12 and 13.56 MHz have been used. The top of the discharge is normally a solid, grounded aluminum plate forming the boundary condition for the low-field peak effect. This condition determined the height of the tube. In the vertical-probe extension, the top plate is replaced with one that has a 1/8-in. (3.2 mm) diameter hole through which two alumina probe shafts are inserted, one for the probe and the other for the RF-compensation electrode (not shown). Details of the probe design are given in a separate paper.[8]

B. Experimental chamber

Figure 2 shows the aluminum experimental chamber to scale with the helicon source. From its previous use as a plasma processing chamber, the interior sidewall is aluminized, and the exterior sidewall is covered with rows of small, round SmCo magnets for better plasma confinement. There are three horizontal Langmuir probes at ports 1, 2, and 3 equally spaced below the source. Port 1 accesses the plasma close to the exit hole of the source. The probe there is close to the furthest reach of the vertical probe, and the two probes yield the same density at the overlap point. Port 2 is at a convenient level for placement of a substrate. A substrate at port 3 would see more uniform plasma at densities below 10^{11} cm^{-3}.

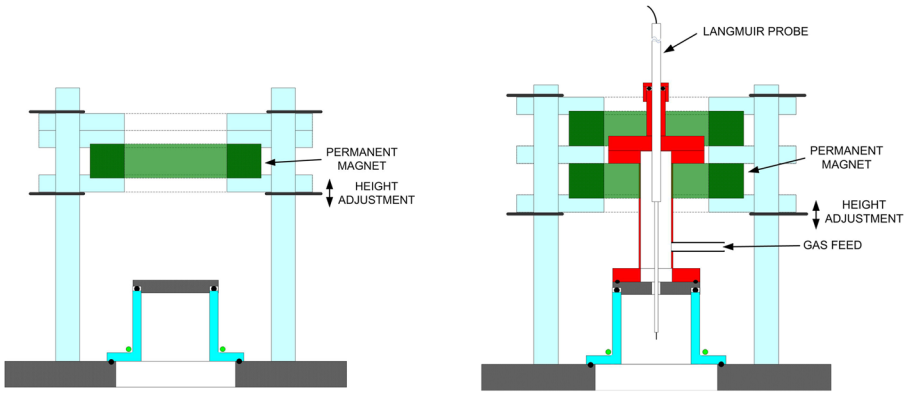

FIG. 1. Diagram of helicon source: (a) simple configuration; (b) with vertical probe extension and second magnet.

C. Design of the discharge tube

Figure 3 shows the dimensions of the tube. The tube radius was chosen by standard pipe sizes and the goal of a small, compact source. The height of the tube was then determined by the condition for a low field peak in density. For this, the HELIC code by Arnush[9] was used. The use of this code was illustrated in a previous paper.[10] The code computes the plasma resistance R (or R_p), which is proportional to the deposition of RF energy for a given antenna current. Since R_p is of the order of 1 Ω, it is important to maximize it to overcome circuit losses. Figure 4 shows calculated curves of R vs. n for various B-fields. It shows that a large gain in loading accrues from raising the frequency to 27.12 MHz; hence, this frequency was used for the first time. Stable operation occurs on the right side of each peak. To obtain high 10^{11} cm^{-3} downstream, we expected n to be in the high 10^{12} cm^{-3} range, which requires high B. This turned out to be incorrect.

The water-cooled antenna is a coil of 1/8-in. (3.2 mm) o.d. copper tube, three turns for 13 MHz and 1 turn for 27 MHz. When cable length is taken into account, manual matching by a standard matching circuit fixes a maximum value for antenna inductance; hence the antenna change for 27 MHz. Details on the inductance limit are given in Ref. 3. Note that the quartz tube is flared out into a "skirt" at the bottom. This is to move the antenna away from the flange on which the tube sits, to prevent induction of large eddy currents in the flange.

D. Diagnostics

Langmuir probes were used exclusively for diagnostics. The horizontal probes are encased in 1/4-in. (6.35 mm) diameter alumina tubes housing the RF chokes and connectors. The probe tip is a 5-mil (0.127 mm) diameter tungsten rod, 0.7-1.2 cm long, centered in a 94-mil (2.39 mm) o.d. alumina tube 2.9 cm in length. An RF-compensation electrode made of 1-mil (25 μm) thick Ni foil is wrapped around the thin tube and connected to the choke chain through a small capacitor. The choke chain consists of one self-resonant choke for 13.56 MHz and three broadly self-resonant chokes in series for 27.12 MHz. The chokes are individually selected. Their impedance varies from 300 to 1000 kΩ at 13.56 MHz and roughly 150-300 kΩ at 27.12 MHz.

The current-voltage ($I-V$) curves were taken by the ESP Mk2® system of Hiden Analytical, Ltd. Each scan

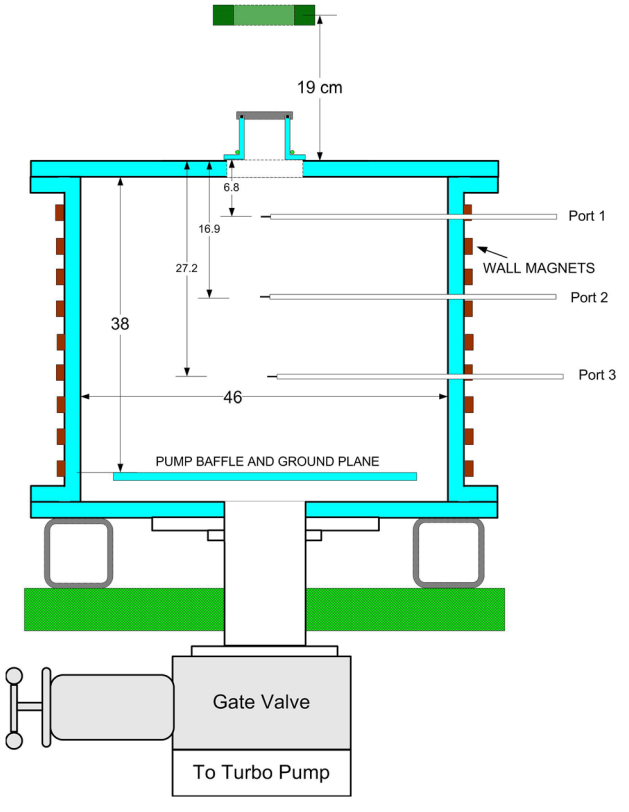

FIG. 2. Diagram of the experimental chamber. Dimensions are in cm.

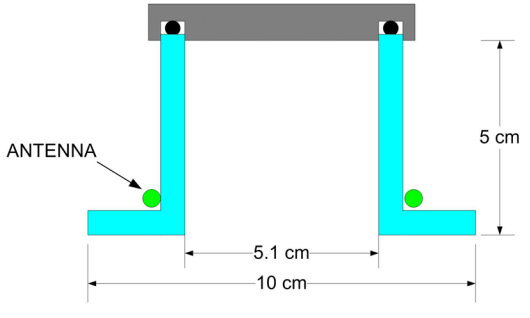

FIG. 3. Nominal dimensions of the discharge tube.

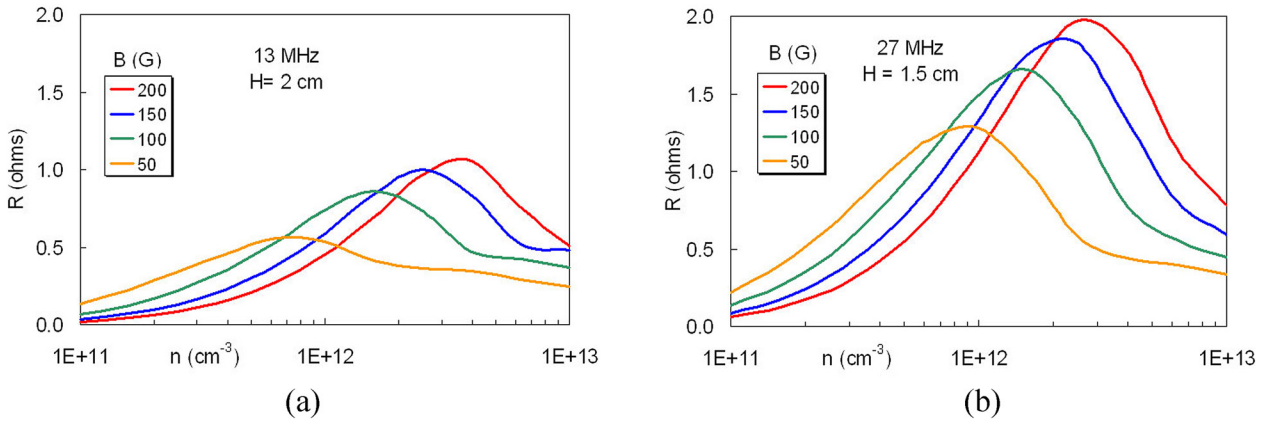

FIG. 4. Plasma resistance calculated for 13 and 27 MHz. The peaks occur at higher n for higher B. Here, H is the antenna distance below the top plate.

consisted of about 200 points from -100 to $\approx +20$ V, taking about 5 s. The $I-V$ curves were analyzed with an Excel program based on Langmuir's Orbital Motion Limited (OML) formula. Each data point shown below was found by fitting its I^2-V plot to a straight line for n, and its $\ln(I_e)$-V plot to another straight line for KT_e, where I_e is the electron current found by subtracting the ion *fit* from I. The electron distribution is almost always consistent with a Maxwellian.

III. MEASUREMENTS

Unless otherwise specified, measurements were made under the standard conditions of 15 mTorr of argon and 400 W of RF. The discharge can be run continuously, but to protect the probes, it is normally turned off as soon as the probe sweep is finished.

A. Downstream profiles at 27.12 MHz

Initially, it was thought that the high densities covered by the right-most curve in Fig. 4(b) could be achieved, and two magnets were used to produce a high field of 200 G at the antenna. In Fig. 5, the axial field strength B_z (B_r is negligible) is shown vs. distance below the magnet. The tube is shown positioned with the antenna at 200 G. Radial profiles in port 1, 6.8 cm below the tube, are shown in Fig. 6. The density is double-peaked, showing edge ionization by the Trivelpiece-Gould (TG) mode. KT_e, however, is peaked at the center, possibly because of neutral depletion, though this could not be confirmed. The TG mode is more strongly peaked at high B, and its visibility indicated that perhaps the B-field was too high for the relatively low density. One magnet was removed to lower the field to about 65 G. For a given n, as seen in Fig. 4, too high a B-field would put the

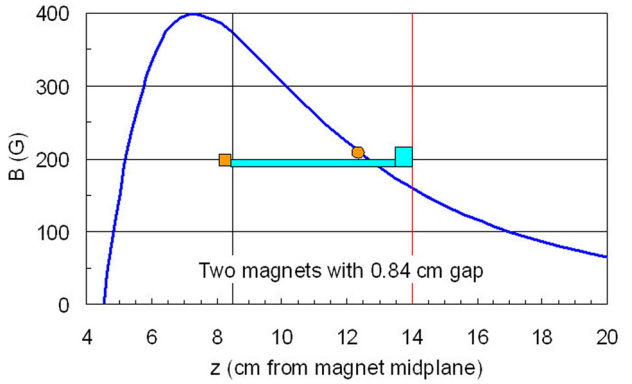

FIG. 5. The remote B-field profile of two magnets, with one possible position of the tube. The much stronger field inside the ring magnets lies to the left and is of opposite sign.

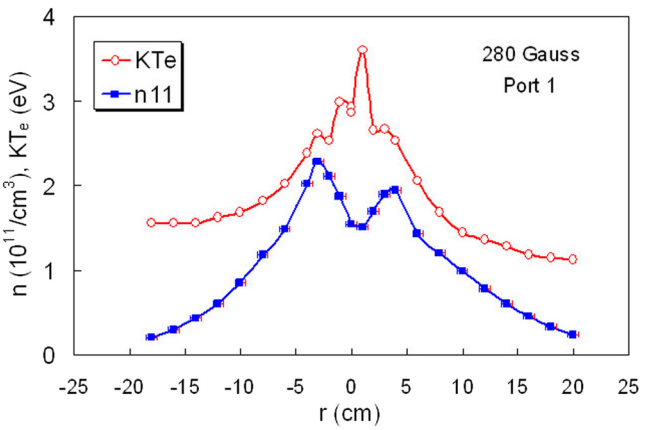

FIG. 6. Profiles of n and KT_e in port 1 at high field. In the graphs n_{11} is density in units of 10^{11} cm^{-3}.

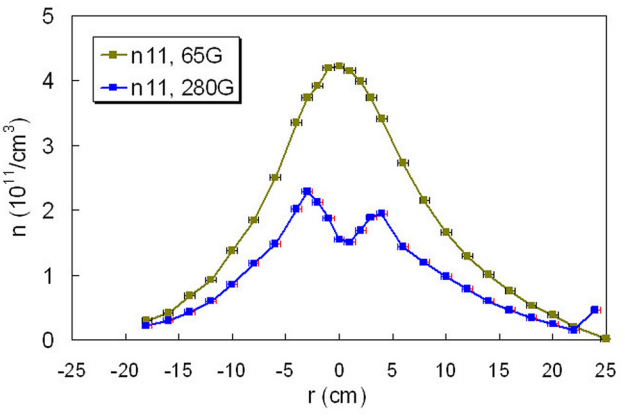

FIG. 7. Density profiles in port 1, showing improvement at lower B-field.

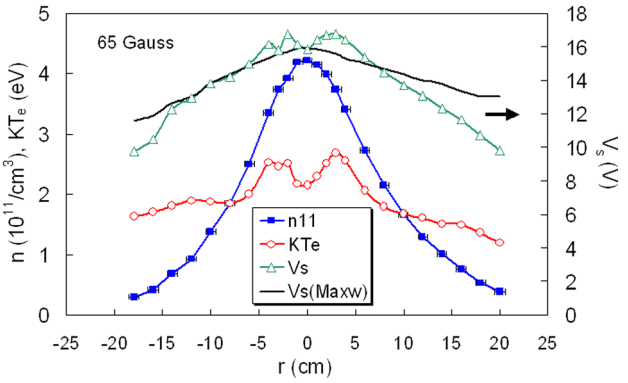

FIG. 8. Profiles of n, KT_e, and V_s in port 1 at low field and 27.12 MHz.

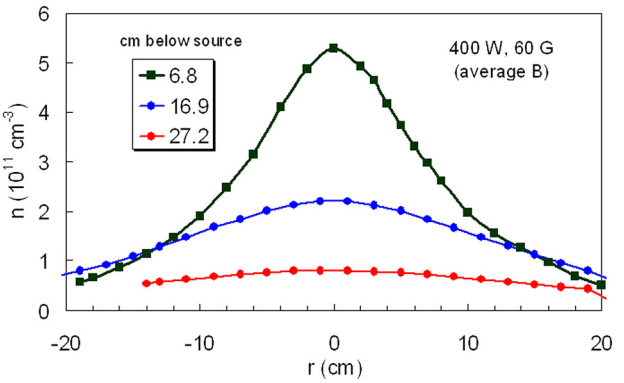

FIG. 10. Density profiles at the three ports after optimization of B.

operating point to the left of the peak in R, which is an unstable regime of operation. Figure 7 shows the great improvement in port 1 density. Figure 8 shows that KT_e is now peaked at the edge due to the TG mode. As explained in Ref. 8, the plasma potential V_s can be obtained from the $\ln(I_e)-V_p$ curve and is also shown in Fig. 8. If electrons are Maxwellian, V_s can also be calculated from the n and KT_e curves using the Boltzmann relation. This yields the solid curve in Fig. 8, which is in fair agreement with direct measurements of V_s.

Figure 9 shows the profiles at ports 2 and 3 after optimization of the B-field (to be shown later). It is seen that the profiles widen by spreading of the field lines and by diffusion as the plasma moves downward. The temperature also decays and becomes more uniform. Also shown in the port 2 plot is a fit to the Bessel function $J_0(r)$ representing the lowest diffusion mode. The edge density does not fall to zero as it does in J_0, presumably due to confinement by the wall magnets. The densities at the three ports are shown together in Fig. 10.

B. Power and pressure scans at 27.12 MHz

The variation of n with RF power P_{rf} is shown for port 2 in Fig. 11(a). The density increases linearly with power as is normal. By comparison, the density inside the discharge, shown in Fig. 11(b), is far from linear. This indicates that ejection of plasma from the discharge is more efficient at high power even though KT_e does not increase with power. The physics of this behavior is not yet understood. Figure 12 compares the power scans at 62 and 280 G in port 1. The lower field is superior, but the 62-G line bends down at the highest P_{rf}, indicating that 62 G is not the optimum field at the high density there. As shown in Fig. 4, the R curve shifts to higher density as B is increased, and B has to be increased to be consistent with the high density at 1000 W. Note that n almost reaches $10^{12}\,\mathrm{cm}^{-3}$ at 1000 W even outside the discharge.

Figure 13 shows a typical pressure scan at 27 MHz. Stable plasmas can be obtained up to 60 mTorr of Ar and beyond. Peak downstream density at port 2 can reach $10^{12}\,\mathrm{cm}^{-3}$ at high pressure. The gas inlet is usually in the large chamber, but top feed into the source can be used when the vertical probe extension is in place. However, we have found no dependence on inlet location. The pressure is measured before discharge initiation. When the plasma is on, the neutrals will be heated and their density will decrease. Note that T_e decreases with pressure, as predicted by theory.

C. Comparison with ICPs

The discharge can be run as an inductively coupled plasma (ICP) with the magnet removed. In the helicon mode, the bright discharge fills the entire tube uniformly, but in the ICP mode, the brightness is higher near the antenna.

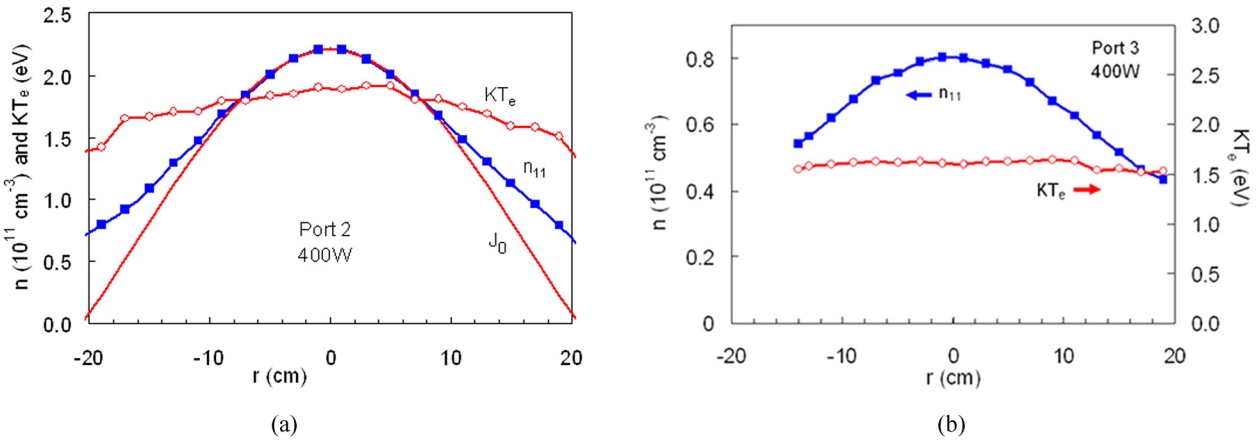

FIG. 9. Profiles of n and KT_e in (a) port 2, 16.9 cm below, and (b) port 3, 27.2 cm below the source. The solid line in (a) is a fit to the Bessel function $J_0(r)$.

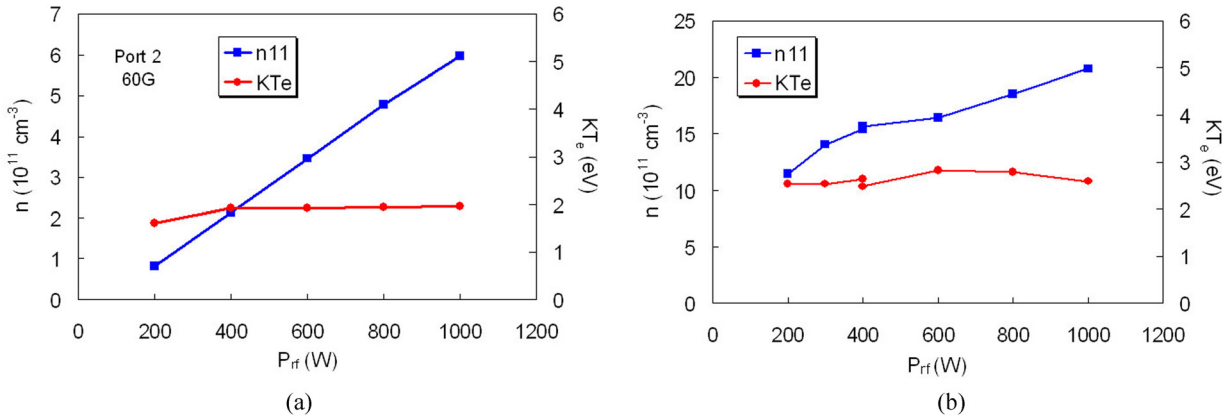

FIG. 11. Powers scans (a) on axis in port 2 and (b) at center inside the discharge tube at 15 mTorr pressure. The two points at 400 W in (b) were taken at the beginning and end of the run, showing reproducibility.

Nonetheless, the downstream density is only slightly lower at 400 W. The helicon's advantage increases with power. Figure 14 compares the densities in ports 1 and 2, and Fig. 15 compares their power scans in port 2. The density advantage of helicons vs. power is shown in Table I.

Another advantage of helicons is its higher plasma resistance R_p. Our algebraic formula[11] for calculating the load (C_L) and tuning (C_T) capacitors in the matching circuit can be used in reverse to calculate the antenna inductance and R_p once C_L and C_T are measured. The difference in R_p's is shown in Fig. 16.

D. Optimization of B-field

One may think that the field of permanent magnets cannot be varied, but the reverse field of ring magnets beyond the stagnation point diverges slowly enough that B can be varied simply by moving the magnet up or down relative to the tube. The magnet mount shown in Fig. 1 is designed for such manual adjustments. In an industrial unit, the mount can be designed to move the magnet by remote control. Tests were made to optimize the peak density at port 2, a convenient location for a substrate, at various RF powers. The magnet heights were converted to B-fields in gauss by using a graph similar to Fig. 5 but drawn for a single magnet. The results are summarized in a complicated Figure 17. The solid lines show the variation of $n(0)$ with B at various powers P_{rf}. The ICP case is at the left ($B = 0$). In the standard 400 W case, n drops for any field greater than ≈60 G. At 200 W, $B < 45$ G is required. At high powers, high density is maintained to higher fields, but there is no advantage going higher than 40 G. The horizontal dotted lines in Fig. 17 show the variation of B between the top and bottom of the tube. Each dotted line is centered on a vertical row of points representing a given magnet height. The shape of the symbol on each dotted line corresponds to the same shape of the data points. At the highest average B of 141 G, the magnet is low, and the field lines are more curved, making B range from 89 to 192 G within the tube. At low B, the magnet is far from the tube, and the field is more uniform. Uniformity, however, may not be important. A smaller magnet closer to the tube could be used to make the source even smaller and lighter.

E. Other optimizations

Although HELIC calculations (Fig. 4(b)) showed that the antenna should be closer to the endplate at 27 MHz than at 13 MHz, moving the single-turn antenna upwards from the bottom did not improve the density. The highest downstream density is always obtained with the antenna closest to the exit aperture. This minimizes internal losses in the tube and is the primary design consideration. With the vertical extension in place, the endplate of the tube can be removed, thus violating the low field peak resonance condition. This does lower the density, but only by 15% at 400 W and less at higher P_{rf}.

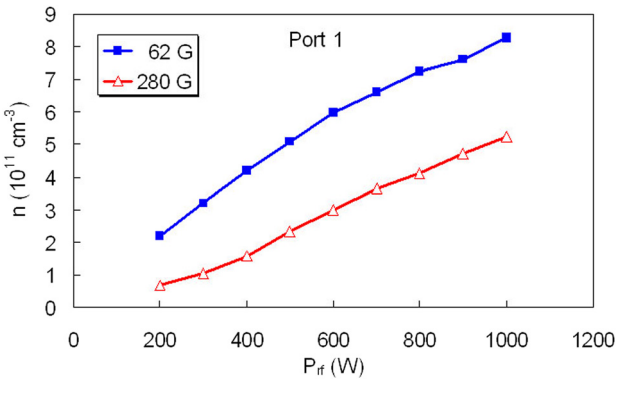

FIG. 12. Power scan in port 1 at high and low B-field.

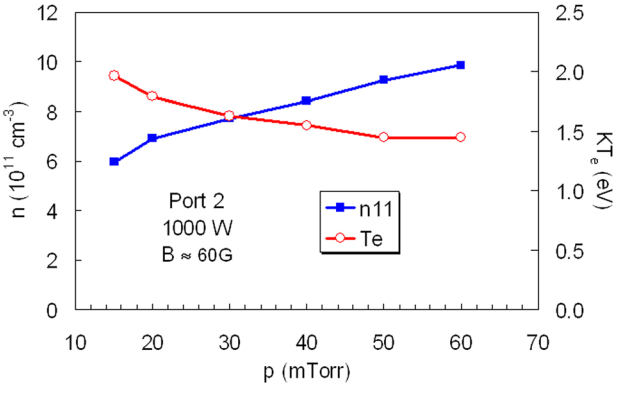

FIG. 13. Pressure scan at 1000 W in port 2.

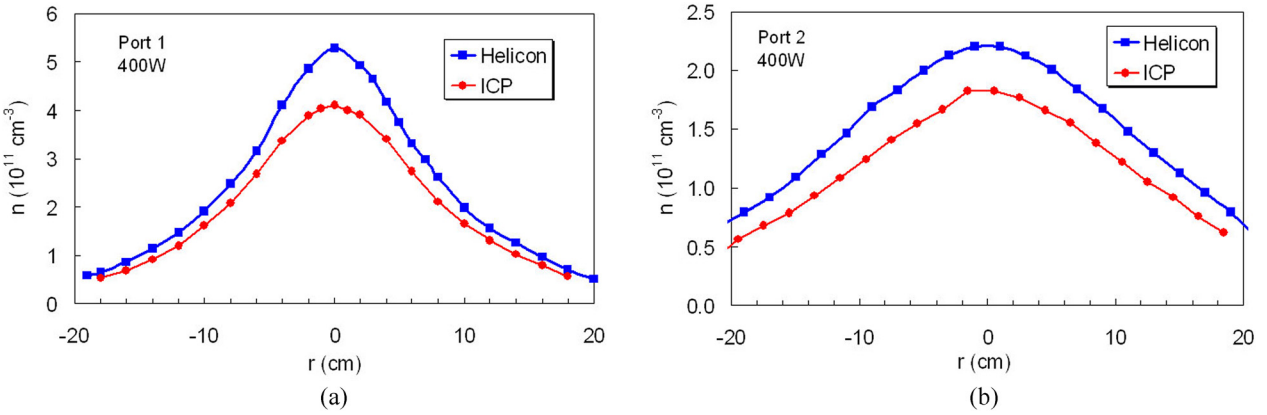

FIG. 14. (a) Port 1 and (b) port 2 density profiles under helicon and ICP operations.

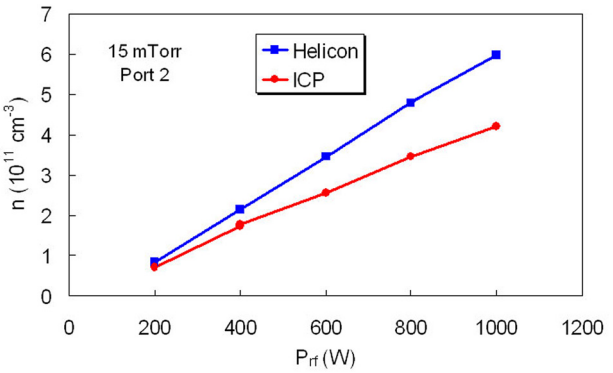

FIG. 15. Comparison of helicon and ICP power scans.

TABLE I. Helicon advantage.

Prf	%
200	16
400	21
600	35
800	38
1000	42

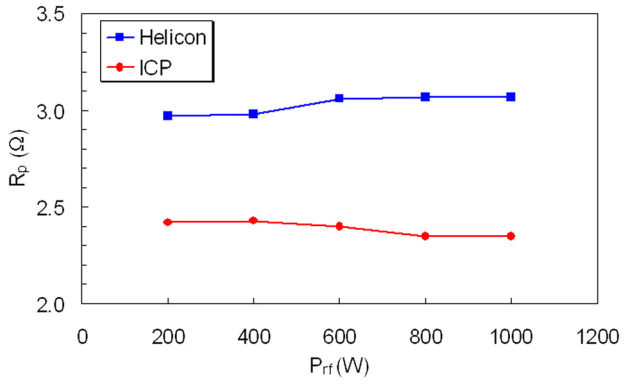

FIG. 16. Plasma loading resistances of helicon and ICP discharges. The zero is suppressed.

F. Operation at 13.56 MHz

To show that 27.12 MHz is more suitable for our small discharge tube (Fig. 4), we reverted to the 13.56 MHz power supply used for the 8-tube Medusa 2 experiment.[3] To our surprise, the lower frequency produced higher density. This is shown in the power scans (Fig. 18) and density profiles (Fig. 19(a)) in port 2. The electron temperature (Fig. 19(b)), however, was unchanged. The optimal magnet position at 400 W was essentially the same as at 27 MHz.

The power scan in port 2 at 13 MHz (Fig. 20(a)) is linear as in Fig. 11(a) for 27 MHz. The pressure scan (Fig. 20(b))

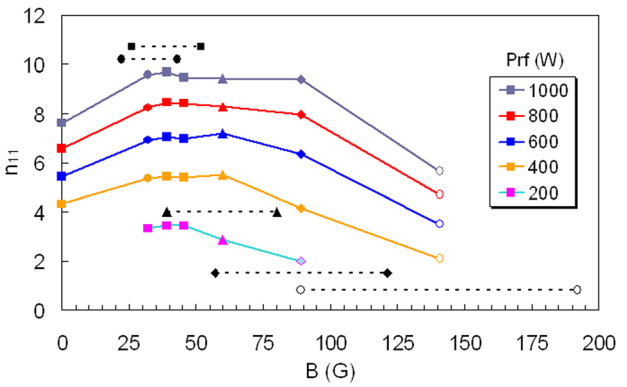

FIG. 17. Variation of port 2 center density with B-field and RF power. Explanation in text.

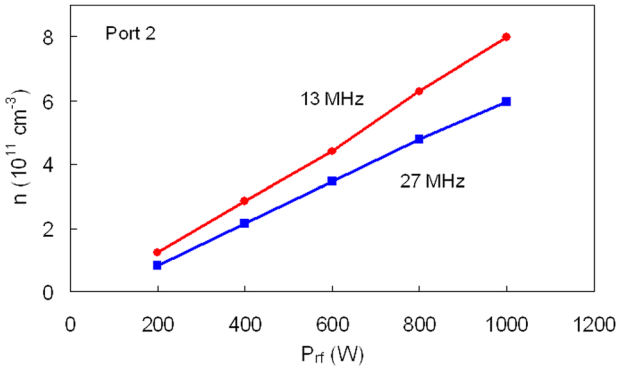

FIG. 18. Power scans in port 2 at 13 and 27 MHz.

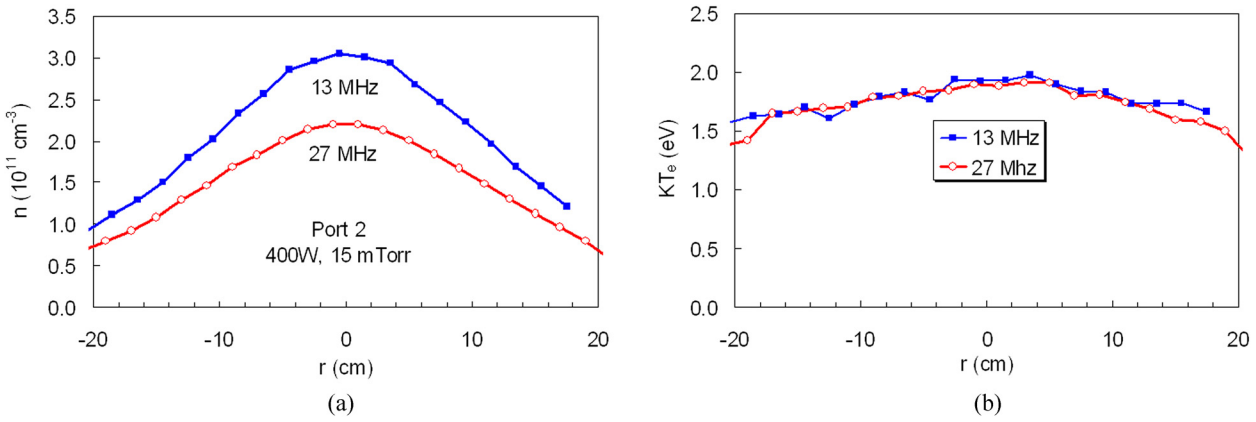

FIG. 19. Radial profiles of (a) density and (b) KT_e in port 2 at 13 and 27 MHz.

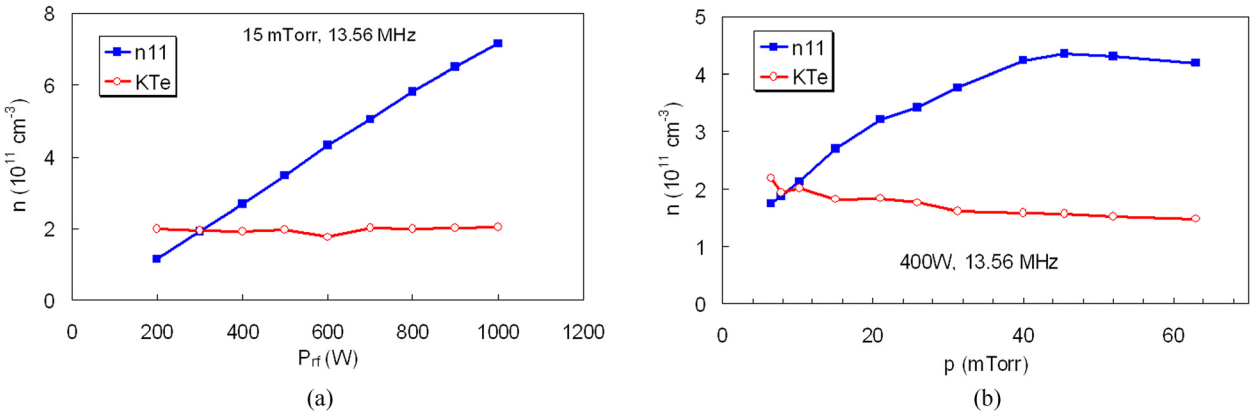

FIG. 20. (a) Power and (b) pressure scans of n and T_e in port 2 at 13.56 MHz.

was taken at 400 W and shows saturation at high pressure. This did not happen at 27 MHz (Fig. 11(b)) because that was taken at 1000 W, so that there is no direct comparison. However, the pressure scan *inside* the tube (Fig. 21) does not level off even at 400 W, and n reaches $5 \times 10^{12}\,\mathrm{cm}^{-3}$ at 1000 W, somewhat higher than was achievable at 27 MHz. The inverse dependence of T_e with pressure is clearly shown in Fig. 21.

A disadvantage of 13 MHz is that the plasma does not break down below 7 mTorr. In previous experiments at that frequency, two leak valves were used, one set for 30-40 mTorr and the other for the operating pressure of 15-20 mTorr. After breakdown, the valves were switched. At 27 MHz, however, the plasma will breakdown below 1 mTorr. This difference is not understood.

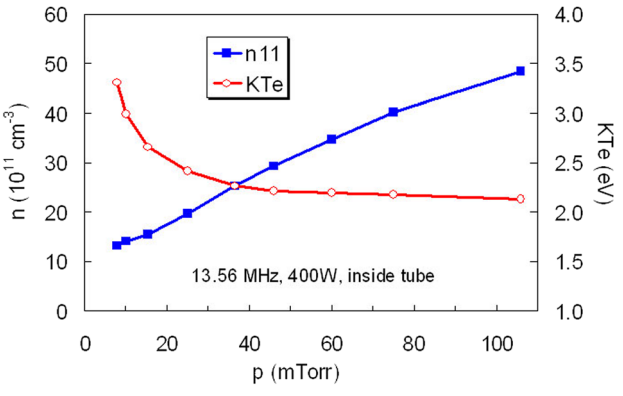

FIG. 21. Pressure scan at 13 MHz inside the discharge tube.

G. Stability

The discharge has no low-frequency drift-wave type instabilities because the ions are unmagnetized and can short-circuit cross-field potentials. To show this, Fig. 22(a) is a dc-coupled oscilloscope trace of the RF-compensated probe current with no zero offset. Fig. 22(b) is an ac-coupled expansion of the current at 5 μs/div. There are no fluctuations in the 10-100 kHz regime but only a slow decrease of the current due to a drop in the density of neutrals as they heat up. The "noise" is a pure sine wave at 27.12 MHz.

IV. DISCUSSION

Contrary to expectations, n is not lower but higher, by about 30%, at 13 MHz than at 27 MHz. The question is why. The reason may simply be a difference in antenna coupling. A three-turn antenna is used at 13 MHz to fit the range of inductance compatible with a two-capacitor matching circuit. At 27 MHz, a one-turn antenna has to be used, and this may

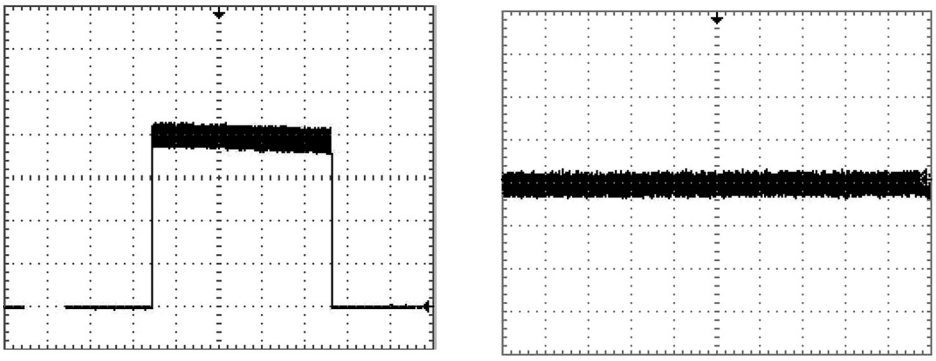

(a) (b)

FIG. 22. Oscilloscope traces of saturation ion current at $V_p = -95$ V at 400 W, 15 mTorr, 27 MHz. Sweep speeds are (a) 1 s/div and (b) 5 μs/div.

couple less efficiently to the plasma. Thus, the reason may be related to practical engineering and not to helicon physics at all.

At either frequency, the small tube is a very efficient injector of plasma. The amount of plasma in the tube is surprisingly small compared with the amount with which it fills the chamber in steady state. The small source supplies the diffusion losses to the large surface area of the chamber. The average density inside the tube has been calculated from the z-profile measured with the vertical probe,[8] together with an r-profile calculated from theory[12] (it could not be measured). The result is $\langle n_{11} \rangle = 3.9 \times 10^{11}\,\mathrm{cm}^{-3}$ *inside* the tube. Compared with this, the average density is $1.2 \times 10^{11}\,\mathrm{cm}^{-3}$ at port 2 computed from a curve such as that in Fig. 9. Thus, the downstream density is only about a factor of 3 less than that in the tube, although the plasma radius is 21 cm downstream vs. only 2.5 cm in the tube. Although we do not have a z-profile inside the large chamber to calculate the total wall losses, we find that a single small source with a peak density below $4 \times 10^{12}\,\mathrm{cm}^{-3}$ can cover a substrate with plasma well above $10^{11}\,\mathrm{cm}^{-3}$. The *flux* of plasma will be measured in future work. In practice, one would use an array of sources designed with the single-source data presented here.

Although helicon theory in uniform cylinders with TG-mode coupling is well in hand, it is inadequate for designing and explaining helicon plasma injectors. In principle, particle-in-cell codes can calculate plasma profiles in any geometry, but they cannot easily cover a large number of cases the way the HELIC code can as in Fig. 4. More importantly, they have not so far included the important Simon short-circuit effect as described in Ref. 12. To illustrate the failure of theory, we have used HELIC to calculate the low-field peak in plasma resistivity R for the exact measured dimensions of the tube and the antenna when the magnet is at the optimum height. In Fig. 23, the solid lines are for the highest field in the tube, 80 G, and the dashed lines for the lowest, 39 G. The red curves (color online) are for 27 MHz and the blue ones for 13 MHz. The shaded area is the range of densities inside the tube. We see that the shaded area does not cover a good range of negative slope in R if B = 80 G. It does cover an acceptable range if B = 39 G, where the antenna is. However, R is very low, of order 0.4 Ω. This is very different from Fig. 4, which was used for design with the belief that n inside the tube would be close to $10^{13}\,\mathrm{cm}^{-3}$. In the initial design, we did not know that the helicon source would be such an efficient ejector of plasma that n inside the tube would be so low, and also we could not account for the axial nonuniformity of B with the theory available. The experiment showed that the optimal conditions correspond to the poor-looking curves of Fig. 23. Also, the measured value of R was close to 3 Ω rather than to 0.4 Ω. Thus, theory served only as a very rough guide to the experiment.

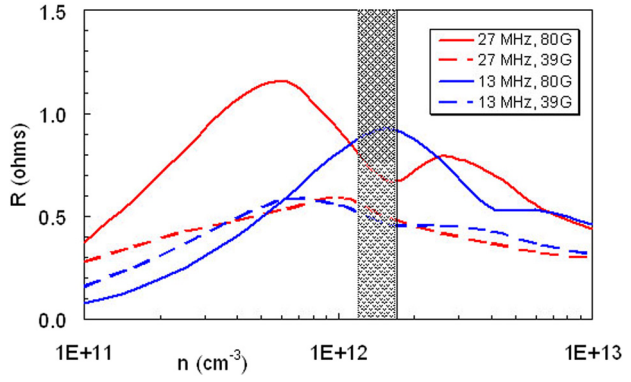

FIG. 23. HELIC calculations of plasma resistivity for the range of B-fields and densities inside the tube when the downstream density is optimal.

In conclusion, a very compact, economical, and efficient source of plasma has been characterized. Though theory provided the initial impetus, nothing can replace experiment.

[1]F. F. Chen, U.S. patent 8,179,050 (15 May 2012).
[2]F. F. Chen, Phys. Plasmas **10**, 2586 (2003).
[3]F. F. Chen and H. Torreblanca, Phys. Plasmas **16**, 057102 (2009).
[4]C. Charles, Plasma Sources Sci. Technol. **16**, R1 (2007).
[5]K. Takahashi, K. Oguni, H. Yamada, and T. Fujiwara, Phys. Plasmas **15**, 084501 (2008).
[6]K. Takahashi and T. Fujiwara, Appl. Phys. Lett. **94**, 061502 (2009).
[7]K. Takahashi, Y. Igarashi, and T. Fujiwara, Appl. Phys. Lett. **97**, 041501 (2010).
[8]F. F. Chen, J. D. Evans, and W. Zawalski, Plasma Sources Sci. Technol. **21**, 055002 (2012).
[9]D. Arnush, Phys. Plasmas **7**, 3042 (2000).
[10]F. F. Chen, IEEE Trans. Plasma Sci. **36**, 2095 (2008).
[11]F. F. Chen, "Helicon plasma sources," in *High Density Plasma Sources*, edited by O. A. Popov (Noyes, Park Ridge, NJ, 1995), Chap. 1, p. 60.
[12]D. Curreli and F. F. Chen, Phys. Plasmas **18**, 113501 (2011).